

Neutrino-Induced Nucleosynthesis in Helium Shells of Early Core-Collapse Supernovae

Projjwal Banerjee^{1,a}, Yong-Zhong Qian^{1,5}, Alexander Heger^{2,5}, and Wick Haxton^{3,4}

¹*School of Physics and Astronomy, University of Minnesota, Minneapolis, Minnesota 55455, USA*

²*Monash Center for Astrophysics, School of Physics and Astronomy, Monash University, Victoria 3800, Australia*

³*Department of Physics, University of California Berkeley, Berkeley, California 94620, USA*

⁴*Lawrence Berkeley National Laboratory, Berkeley, California 94620, USA*

⁵*Center for Nuclear Astrophysics, INPAC, Department of Physics and Astronomy, Shanghai Jiao Tong University, Shanghai 200240, People's Republic of China*

Abstract. We summarize our studies on neutrino-driven nucleosynthesis in He shells of early core-collapse supernovae with metallicities of $Z \lesssim 10^{-3} Z_{\odot}$. We find that for progenitors of $\sim 11\text{--}15 M_{\odot}$, the neutrons released by ${}^4\text{He}(\bar{\nu}_e, e^+ n){}^3\text{H}$ in He shells can be captured to produce nuclei with mass numbers up to $A \sim 200$. This mechanism is sensitive to neutrino emission spectra and flavor oscillations. In addition, we find two new primary mechanisms for neutrino-induced production of ${}^9\text{Be}$ in He shells. The first mechanism produces ${}^9\text{Be}$ via ${}^7\text{Li}(n, \gamma){}^8\text{Li}(n, \gamma){}^9\text{Li}(e^- \bar{\nu}_e){}^9\text{Be}$ and relies on a low explosion energy for its survival. The second mechanism operates in progenitors of $\sim 8 M_{\odot}$, where ${}^9\text{Be}$ can be produced directly via ${}^7\text{Li}({}^3\text{H}, n_0){}^9\text{Be}$ during the rapid expansion of the shocked He-shell material. The light nuclei ${}^7\text{Li}$ and ${}^3\text{H}$ involved in these mechanisms are produced by neutrino interactions with ${}^4\text{He}$. We discuss the implications of neutrino-induced nucleosynthesis in He shells for interpreting the elemental abundances in metal-poor stars.

1 Introduction

Observations of the chemical composition in metal-poor stars provide important clues for the source of metal enrichment in the early Galaxy. In this regard, extremely metal-poor (EMP) stars with $[\text{Fe}/\text{H}] \equiv \log(\text{Fe}/\text{H}) - \log(\text{Fe}/\text{H})_{\odot} \lesssim -2.5$ are especially useful as they sample gases polluted by just a few nucleosynthetic events. With a growing number of observational studies on EMP stars, it has now become clear that neutron-capture elements were present in the early Galaxy, where only stars more massive than $\sim 8 M_{\odot}$ that end their lives as core-collapse supernovae (CCSNe) could have contributed [1]. The abundance patterns observed in EMP stars show large variations. Some stars have abundance patterns similar to the solar rapid neutron-capture (r) process distribution and others have patterns similar to the slow neutron-capture (s) process distribution or to a mixture of r and s process distributions [2]. This suggests a variety of neutron-capture processes operated in the early Galaxy. EMP stars with s -process signatures are thought to have experienced surface pollution by a binary

^ae-mail: banerjee@physics.umn.edu

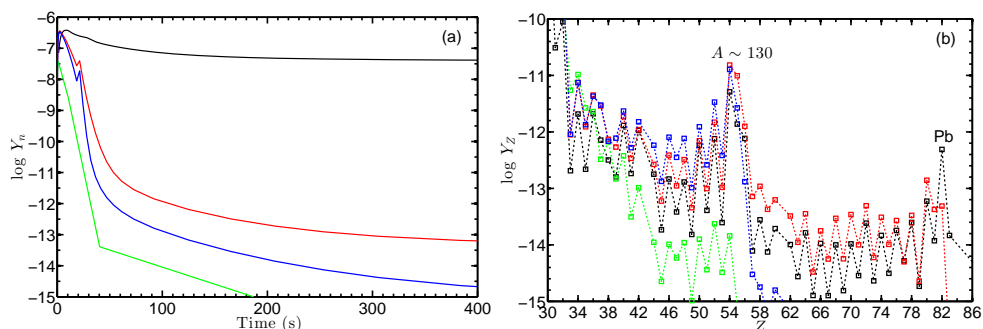


Figure 1. (a) Evolution of neutron abundance Y_n with time for a typical zone in the outer He shell for y11H.1 (black), u11*H.1 (red), u11H.1 (blue), and v11H.1 (green). (b) Final elemental abundance pattern produced by y11H.1 (black), u11*H.1 (red), u11H.1 (blue), and v11H.1 (green).

companion during the latter’s evolution on the asymptotic giant branch. However, the astrophysical site of r -process in the early Galaxy and the mechanism for producing a mixture of r and s patterns, especially in stars that are not in binary systems, are still uncertain. We revisit a mechanism for producing neutron-capture elements in the early Galaxy originally proposed by Epstein, Colgate, and Haxton (ECH) [3]. We show that in metal-poor progenitors with metallicities of $Z \lesssim 10^{-3} Z_\odot$ and masses of $\sim 11\text{--}15 M_\odot$, a modified version of the ECH mechanism can lead to production of nuclei with mass numbers up to $A \sim 200$ [4]. We identify a related mechanism for producing the rare light nucleus ^9Be that previously had been thought to be produced exclusively by interactions between Galactic cosmic rays (GCRs) and nuclei in the interstellar medium [5, 6]. Furthermore, ^9Be can be synthesized by neutrino-induced reactions in He shells of more compact progenitors of $\sim 8\text{--}10 M_\odot$. We find that ^9Be produced by the above mechanisms can account for the linear relationship of Be with primary products of CCSNe, e.g., O, Mg, Ti, and Fe, as observed at low metallicities [7].

2 Neutrino-Induced Neutron-Capture Process in the He Shell

The ECH mechanism was proposed as a possible scenario for the r process in CCSNe. The main idea is that neutrinos emitted during a CCSN will produce neutrons in neutral-current reactions with ^4He via $^4\text{He}(\nu, \nu' n)^3\text{He}(n, p)^3\text{H}(^3\text{H}, 2n)^4\text{He}$ and $^4\text{He}(\nu, \nu' p)^3\text{H}(^3\text{H}, 2n)^4\text{He}$. As neutrons cannot capture on ^4He , they will instead be absorbed with high efficiency by trace quantities of ^{56}Fe present from initial birth material of the star. As the number of neutrons generated by this primary neutrino-driven mechanism can be computed reasonably well, it can be shown that the neutron/seed ratio needed for a successful r process can be achieved in metal-poor He shells. It was pointed out in Ref. [8] however, that this mechanism would only be viable in CCSNe from low-metallicity compact stars and even there poisons such as ^{12}C may inhibit the r process. We revisit this scenario by performing detailed nucleosynthesis calculations with the hydrodynamic code KEPLER [9, 10]. We use the same code to evolve progenitor models and treat the effects of the CCSN shock. Progenitors investigated have metallicities of $[Z] \equiv \log(Z/Z_\odot) = -5$ (denoted by “y” for “hyper-metal-poor”), -4 (“u” for “ultra-metal-poor”), and -3 (“v” for “very-metal-poor”) and masses of $11\text{--}15 M_\odot$. The progenitor models are labelled by their metallicity and mass in units of M_\odot . For example, u11 refers to a progenitor with metallicity “u” of $11 M_\odot$. We study the sensitivity of the final abundance pattern to neutrino spectra, flavor oscillations, explosion energy, and progenitor metallicity.

The progenitor models y11, y15, u11, u15, v11, and v15 are generated using the most recent version of KEPLER with a full reaction network to track the evolution of a massive star from birth

till right before core collapse. We also consider modified models u11* and u15*, which have the abundances of ^{28}S and ^{32}Si in the He shell reduced by a factor of ~ 10 to match similar models in Ref. [11]. The explosion is modeled by driving a piston through the collapsing progenitor and then following the propagation of the shock wave [9]. The nucleosynthesis due to shock heating and that due to neutrino emission from the protoneutron star (PNS) are followed using the full reaction network. The neutrino luminosity is taken to be $L_\nu(t) = L_\nu(0) \exp(-t/\tau_\nu)$ for each of the six species, with $L_\nu(0) = 16.7 \text{ B/s}$ ($1 \text{ B} \equiv 10^{51} \text{ erg}$) and $\tau_\nu = 3 \text{ s}$, which amounts to a total energy of 300 B emitted in neutrinos. We adopt Fermi-Dirac neutrino spectra with zero chemical potential and constant temperatures T_{ν_e} , $T_{\bar{\nu}_e}$, and $T_{\nu_x} = T_{\bar{\nu}_x}$ ($x = \mu, \tau$). We take $(T_{\nu_e}, T_{\bar{\nu}_e}, T_{\nu_x}) = (4, 5.33, 8) \text{ MeV}$ (H) and $(3, 4, 6) \text{ MeV}$ (S), which represent the harder and softer spectra obtained from earlier (e.g., [12]) and more recent [13, 14] neutrino transport calculations, respectively.

Similar to Ref. [4], the site for the neutrino-induced neutron-capture process is the outer He shell where the composition is nearly pure ^4He and mass fractions of poisons such as ^{12}C , ^{14}N , and ^{16}O are so low that they capture very few neutrons. For the models considered here, this corresponds to a typical radius of $\sim 10^{10} \text{ cm}$, a pre-shock temperature of $\sim 9 \times 10^7 \text{ K}$ and density of $\sim 50 \text{ g/cm}^3$. We calculate neutrino-induced nucleosynthesis both before and after the arrival of the shock. The neutrino spectra in the outer He shell should differ from the initial spectra at the PNS surface due to flavor oscillations associated with the atmospheric neutrino mass splitting $|\delta m_{13}^2| \sim 2.4 \cdot 10^{-3} \text{ eV}^2$ (see e.g., [15, 16]): the neutrinos experience a level crossing before they reach the He shell. For the inverted neutrino mass hierarchy (IH), this results in almost full $\bar{\nu}_e \leftrightarrow \bar{\nu}_x$ conversion and consequently an enhanced charged-current rate for $^4\text{He}(\bar{\nu}_e, e^+n)^3\text{H}$. This resulting increase in neutron production is helpful in achieving the necessary neutron/seed ratio [4]. In contrast, for the normal neutrino mass hierarchy (NH), the rate of $^4\text{He}(\nu_e, e^-p)^3\text{He}$ is increased, producing more ^3He to dominate neutron capture, making an r -process impossible. So the NH precludes an efficient neutron-capture process. We explore the case of full $\bar{\nu}_e \leftrightarrow \bar{\nu}_x$ interconversion as well as the case where flavor oscillations are ignored. We also explore a range of explosion energies $E_{\text{expl}} = 0.1\text{--}1 \text{ B}$. The nucleosynthesis calculations are labelled by the progenitor model, the neutrino spectra, and the explosion energy in units of B, with e.g., u8.1H.1 indicating progenitor model u8.1, the harder neutrino spectra H, and $E_{\text{expl}} = 0.1 \text{ B}$. Calculations including $\bar{\nu}_e \leftrightarrow \bar{\nu}_x$ oscillations are denoted by a bar above the H or S.

We find that the highest He-shell neutron abundance and thus the most favorable conditions for an efficient neutron-capture process are obtained with a hard spectra with oscillations for the IH. The neutron abundances Y_n for $11 M_\odot$ progenitors of different metallicities are shown in Fig. 1a. We find that the neutral-current reactions $^4\text{He}(\nu, \nu'n)^3\text{He}$ are ineffective in producing neutrons as they are immediately recaptured via $^3\text{He}(n, p)^3\text{H}$. In addition, the potential neutron-producing reaction $^3\text{H}(^3\text{H}, 2n)^4\text{He}$ is ineffective at the temperatures in the outer He shell. Instead, neutrons are primarily produced by the charged-current reaction $^4\text{He}(\bar{\nu}_e, e^+n)^3\text{H}$. While this production occurs over the $\sim 5\text{--}6 \text{ s}$ period, the neutron-capture process takes place over $\sim 40\text{--}500 \text{ s}$, producing nuclei up to $A \sim 200$. Both ^7Li and ^8Li are produced *in situ* as a result of neutrino reactions and act as important poisons. The nucleus ^7Li is produced by $^4\text{He}(^3\text{H}, \gamma)^7\text{Li}$, where ^3H is made by $^4\text{He}(\bar{\nu}_e, e^+n)^3\text{H}$ and $^4\text{He}(\nu, \nu'p)^3\text{He}$. The nucleus ^8Li is produced by neutron capture on ^7Li . Enough ^9Be is produced via $^7\text{Li}(n, \gamma)^8\text{Li}(n, \gamma)^9\text{Be}$ to account for the ^9Be observed in metal-poor stars [17]. This is discussed in more detail in the next section.

For the y11H.1 model, neutrons are never depleted, which allows neutron capture to last for $\sim 500 \text{ s}$ before the neutron density becomes too low. Such a long timescale causes a considerable amount of Pb to be formed well after 100 s. In addition, availability of high neutron density for $\sim 500 \text{ s}$ allows capture on seeds such as Si, S, Ca, and Ti to contribute to the production of nuclei up to $A \gtrsim 130$. This is unique to the y11H.1 model and is not seen in other models where neutrons are

Table 1. Yields of Be, Sr, and Ba in M_{\odot} [$X(Y) \equiv X \cdot 10^Y$] and the corresponding [Sr/Ba] with $\log(\text{Sr/Ba})_{\odot} = 0.70$

Model	Be	Sr	Ba	[Sr/Ba]
y11 $\overline{\text{H}}$.1	1.48(−8)	3.02(−10)	1.14(−9)	−1.09
y11 $\overline{\text{H}}$.3	7.90(−9)	2.35(−10)	3.21(−10)	−0.65
y15 $\overline{\text{H}}$.1	1.07(−8)	3.43(−11)	1.05(−10)	−1.00
y15 $\overline{\text{H}}$.3	1.01(−9)	6.91(−11)	1.40(−10)	−0.82
u11* $\overline{\text{H}}$.1	1.20(−8)	6.50(−10)	1.87(−9)	−0.97
u11* $\overline{\text{H}}$.3	2.48(−9)	5.70(−10)	1.90(−9)	−1.03
u15* $\overline{\text{H}}$.1	2.44(−9)	1.32(−10)	4.86(−11)	−0.08
u15* $\overline{\text{H}}$.3	8.46(−10)	1.22(−10)	9.50(−11)	−0.40
u11 $\overline{\text{H}}$.1	2.72(−9)	5.99(−10)	1.95(−10)	−0.02
u11 $\overline{\text{H}}$.3	7.13(−10)	4.92(−10)	1.84(−10)	−0.09
u15 $\overline{\text{H}}$.1	9.92(−10)	2.18(−10)	3.27(−12)	1.31
u15 $\overline{\text{H}}$.3	2.23(−10)	3.34(−10)	7.33(−12)	1.14

depleted within $\lesssim 100$ s. For the u* models, hard spectra with $\bar{\nu}_e \leftrightarrow \bar{\nu}_x$ oscillations are required for the nuclear flow to reach $A \sim 200$ (Fig. 1b) but hard spectra without oscillations can reach $A \sim 130$. For the u models ($[Z] = -4$), ^{28}Si and ^{32}S start to become important poisons, competing with ^{56}Fe for the neutrons. In this case, the flow can still reach $A \sim 130$ for hard neutrino spectra with $\bar{\nu}_e \leftrightarrow \bar{\nu}_x$ oscillations. As can be seen from Fig. 1b, neutron capture starts to shut off for the v11 and v15 models when the metallicity reaches $[Z] = -3$.

3 Neutrino-Induced Production of ^9Be in the He Shell

The neutrino-induced neutron-capture process discussed above can also lead to ^9Be synthesis [17]. In addition to neutron capture mainly by ^{56}Fe leading to production of nuclei up to $A \sim 200$, ^9Be is made by a “mini- r process” through $^7\text{Li}(n, \gamma)^8\text{Li}(n, \gamma)^9\text{Li}(e^- \bar{\nu}_e)^9\text{Be}$. In this case, ^7Li and ^8Li act as poisons for the main neutron-capture process but serve as the seeds for ^9Be production. Most of the ^9Be is produced before the arrival of the shock at temperatures $T \lesssim 10^8$ K where the newly-synthesized ^9Be survives. The ^9Be production ceases at shock arrival, which produces temperatures $\gtrsim 2 \times 10^8$ K where $^9\text{Be}(p, ^4\text{He})^6\text{Li}$ and $^9\text{Be}(p, d)^4\text{He}$ can destroy part of the ^9Be . Thus the final ^9Be yield is sensitive to the shock temperature, and hence, the explosion energy. For $E_{\text{expl}} \gtrsim 3$ B, most of the ^9Be is destroyed. In addition, as in the main neutron-capture process, ^9Be production is sensitive to the neutrino spectra, becoming most efficient for hard spectra with oscillations ($\overline{\text{H}}$ models). However, as only two neutrons need to be captured, models with hard spectra without oscillations (H models) and soft spectra with oscillations ($\overline{\text{S}}$ models) are also able to produce substantial amounts of ^9Be . As in the neutrino-induced neutron-capture process, ^9Be production in the He shell ceases for metallicities of $[Z] \gtrsim -3$.

There is a second He-shell neutrino-driven mechanism for producing ^9Be that operates in progenitors with masses of $\sim 8\text{--}9.6 M_{\odot}$, which are near the lower limit for producing a CCSN. Such progenitors are compact, with a very thin He shell and a steeply-falling density profile outside the core. The structure is quite different from that found in progenitors of $\gtrsim 11 M_{\odot}$: the He shell of a progenitor of $\sim 8 M_{\odot}$ is located at a radius of $\sim 10^9$ cm, ten times closer to the core than in an $11 M_{\odot}$ progenitor. As a result, the shock reaches the He shell within ~ 1 s. The peak post-shock temperature reaches $\sim 8 \times 10^8$ K, which destroys all of the ^9Be produced before the arrival of the shock. Due to the

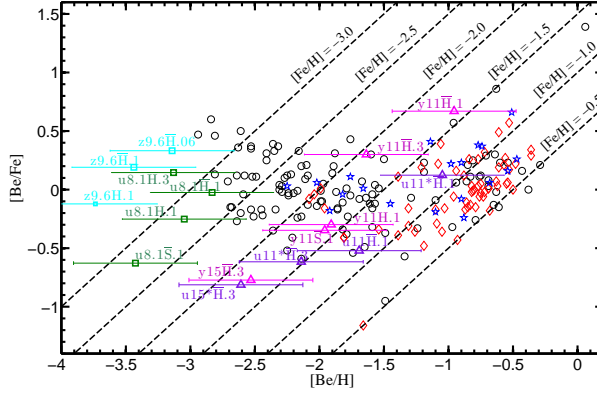


Figure 2. Comparison of [Be/H] and [Be/Fe] from models with data from [7] (black circles), [18] (red diamonds), and [19] (blue stars). The z models correspond to progenitors with zero metallicity.

compact structure however, as the shocked He-shell material expands, the temperature drops below 2×10^8 K within ~ 4 s and destruction of ${}^9\text{Be}$ via ${}^9\text{Be}(p, {}^4\text{He}){}^6\text{Li}$ and ${}^9\text{Be}(p, d)2{}^4\text{He}$ is effectively turned off. At this stage, the He shell is still close to the PNS and is still irradiated by neutrinos, which results in the breakup of ${}^4\text{He}$ via ${}^4\text{He}(\nu, \nu'n){}^3\text{He}$, ${}^4\text{He}(\nu, \nu'p){}^3\text{H}$, and ${}^4\text{He}(\bar{\nu}_e, e^+n){}^3\text{H}$. Then ${}^9\text{Be}$ is made from the breakup products via ${}^4\text{He}({}^3\text{H}, \gamma){}^7\text{Li}({}^3\text{H}, n_0){}^9\text{Be}$. It is important to note that the above production of ${}^9\text{Be}$ also happens in more massive progenitors of $\gtrsim 11 M_\odot$, but in this case all the ${}^9\text{Be}$ produced is destroyed by the shock. Due to the slower expansion in these progenitors, by the time the temperature in the inner He shell drops below 2×10^8 K at ~ 25 s, neutrino emission by the PNS has effectively ceased. Thus the fast expansion due to the sharp density gradient in low-mass progenitors is essential to the production of ${}^9\text{Be}$ via this mechanism. This mechanism is also sensitive to the neutrino spectra due to the high thresholds for the breakup reactions ${}^4\text{He}(\nu, \nu'p){}^3\text{H}$ and ${}^4\text{He}(\bar{\nu}_e, e^+n){}^3\text{H}$. For example, the ${}^9\text{Be}$ yield for u8.1H.1 is ~ 4 times higher than for u8.1S.1.

In Fig. 2 we compare model yields of [Be/H] and [Be/Fe] with the data. The horizontal bar corresponds to the estimated range for the amount of the interstellar medium to mix with the ejecta from each CCSN for the relevant explosion energy [20]. It can be seen that the predicted [Be/H] and [Be/Fe] values from most of the models with hard neutrino spectra agree very well with observations and can account for the observed Be up to [Fe/H] ~ -1 . For the lower explosion energies, some inner ejecta from the 11–15 M_\odot models is likely to fall back onto the PNS so that only a fraction of the Fe produced is ejected while all of the He shell containing the ${}^9\text{Be}$ produced by the first mechanism is ejected. In this case, the predicted [Be/Fe] values in Fig. 2 refer to the lower limits for such models. For the second mechanism of ${}^9\text{Be}$ production that operates in lower-mass CCSNe, all the material is ejected even for low explosion energies. It is possible that the first mechanism operating in 11–15 M_\odot CCSNe can contribute to the Be in stars with [Fe/H] ~ -2 to -1 , whereas the second mechanism operating in lower-mass CCSNe can account for the Be in stars with [Fe/H] $\lesssim -2.5$.

4 Discussion and Conclusions

We have studied neutrino-induced nucleosynthesis in He shells of CCSNe resulting from metal-poor progenitors of both lower masses of ~ 8 –9.6 M_\odot with compact structure and regular masses of 11–15 M_\odot . In regular-mass CCSNe, neutrino interactions with ${}^4\text{He}$ can produce neutrons, which are then captured by Fe seeds to produce heavy nuclei up to $A \sim 200$. Compared to the usual r process, the neutrino-induced neutron-capture process in He shells of metal-poor CCSNe is cold (temperatures of

$\sim 10^8$ K) and slow (timescales ranging to several hundred seconds). This mechanism is sensitive to neutrino spectra, flavor oscillations, and metallicity of the progenitor. Hard spectra with oscillations are required for most models to produce nuclei at and beyond Ba. Depending on the metallicity and neutrino spectra, this mechanism can account for a wide range of [Sr/Ba] from ~ -1 to 1.3 (see Table. 1). This is consistent with the large scatter for [Sr/Ba] observed in metal-poor stars of $[\text{Fe}/\text{H}] \lesssim -2.5$. We find that for typical Sr yields of $\sim (3-8) \times 10^{-10} M_\odot$ mixed with $\sim 10^2-10^3 M_\odot$ of the interstellar medium appropriate for weak explosions [20], various models can account for the [Sr/H] and [Sr/Ba] observed in many of the metal-poor stars with low abundances of neutron-capture elements.

The neutrino-induced neutron-capture process in low-metallicity He shells of $11-15 M_\odot$ CCSNe also results in ^9Be synthesis before the arrival of the shock, which can account for the Be observed in metal-poor stars. In addition, low-mass compact progenitors of $\sim 8-10 M_\odot$ can produce ^9Be in the shocked fast-expanding He shell due to the continuing neutrino irradiation. Both of these mechanisms are consistent with the observed primary nature of Be at low metallicities. Other mechanisms, such as GCR interactions with the interstellar medium, are still required to account for the Be observed at higher metallicities including the solar inventory of Be.

This work was supported in part by the US DOE [DE-FG02-87ER40328 (UM), DE-SC00046548 (Berkeley), and DE-AC02-98CH10886 (LBL)] and by ARC Future Fellowship FT120100363 (AH).

References

- [1] C. Sneden, J.J. Cowan, R. Gallino, *Annu. Rev. Astron. Astrophys.* **46**, 241 (2008)
- [2] T.C. Beers, N. Christlieb, *Annu. Rev. Astron. Astrophys.* **43**, 531 (2005)
- [3] R.I. Epstein, S.A. Colgate, W.C. Haxton, *Phys. Rev. Lett.* **61**, 2038 (1988)
- [4] P. Banerjee, W.C. Haxton, Y.Z. Qian, *Phys. Rev. Lett.* **106**, 201104 (2011)
- [5] R. Ramaty, B. Kozlovsky, R.E. Lingens, H. Reeves, *Astrophys. J.* **488**, 730 (1997)
- [6] N. Prantzos, *Astron. Astrophys.* **542**, A67 (2012)
- [7] A.M. Boesgaard, J.A. Rich, E.M. Levesque, B.P. Bowler, *Astrophys. J.* **743**, 140 (2011)
- [8] S.E. Woosley, D.H. Hartmann, R.D. Hoffman, W.C. Haxton, *Astrophys. J.* **356**, 272 (1990)
- [9] T.A. Weaver, G.B. Zimmerman, S.E. Woosley, *Astrophys. J.* **225**, 1021 (1978)
- [10] T. Rauscher, A. Heger, R.D. Hoffman, S.E. Woosley, *Nucl. Phys. A* **718**, 463 (2003)
- [11] S.E. Woosley, A. Heger, T.A. Weaver, *Rev. Mod. Phys.* **74**, 1015 (2002)
- [12] S.E. Woosley, J.R. Wilson, G.J. Mathews, R.D. Hoffman, B.S. Meyer, *Astrophys. J.* **433**, 229 (1994)
- [13] L. Hudepohl, B. Müller, H.T. Janka, A. Marek, G.G. Raffelt, *Phys. Rev. Lett.* **104**, 251101 (2010)
- [14] T. Fischer, S.C. Whitehouse, A. Mezzacappa, F.K. Thielemann, M. Liebendörfer, *Astron. Astrophys.* **517**, A80 (2010)
- [15] C. Lunardini, A.Y. Smirnov, *J. Cosm. Astropart. Phys.* **6**, 009 (2003)
- [16] H. Duan, G.M. Fuller, Y.Z. Qian, *Annu. Rev. Nucl. Part. Sci.* **60**, 569 (2010), 1001.2799
- [17] P. Banerjee, Y.Z. Qian, W.C. Haxton, A. Heger, *Phys. Rev. Lett.* **110**, 141101 (2013)
- [18] R. Smiljanic, L. Pasquini, P. Bonifacio, D. Galli, R.G. Gratton, S. Randich, B. Wolff, *Astron. Astrophys.* **499**, 103 (2009)
- [19] K.F. Tan, J.R. Shi, G. Zhao, *Mon. Not. R. Astron. Soc.* **392**, 205 (2009)
- [20] K. Thornton, M. Gaudlitz, H.T. Janka, M. Steinmetz, *Astrophys. J.* **500**, 95 (1998)